

Advection-Dominated Transport Dynamics for Pili and Flagella-Mediated Motile Bacteria in Porous Media

Marc Berghouse^{†,‡}, Lazaro J. Perez[†], Andrew Plymale⁺, Timothy D. Scheibe⁺⁺, & Rishi Parashar^{†,*}

[†] Division of Hydrologic Science, Desert Research Institute, Reno, Nevada, 89512

[‡] Graduate Program of Hydrologic Sciences, University of Nevada, Reno, Reno, Nevada, 89557

⁺ Energy and Environment Directorate, Pacific Northwest National Laboratory, Richland, Washington, 99354

⁺⁺ Earth and Biological Sciences Directorate, Pacific Northwest National Laboratory, Richland, Washington, 99354

Corresponding Author: Rishi Parashar

Email: Marc.Berghouse@dri.edu, Lazaro.Perez@dri.edu, plymale@pnnl.gov,
tim.scheibe@pnnl.gov, Rishi.Parashar@dri.edu*

Phone Number of Corresponding Author: +1 775 673 7496

Author Contributions: R.P. and T.D.S. designed research. L.J.P performed experiments. A.P. cultured bacteria and advised on biological aspects of the experiments. M.B. conducted simulations of microfluidic models and analyzed experimental data. M.B., L.J.P., and R. P. interpreted the modeling results. M.B., L.J.P., R.P., and A.P. wrote the paper.

Competing Interest Statement: The authors declare no competing interests.

Preprint Server: N/A

Keywords: Bacterial Transport, Motility, Porous Media

1 **Abstract**

2 The transport of motile bacteria in porous media is highly relevant to many fields, ranging from ecology to
3 human health. Still, critical gaps remain in our understanding of the impacts of hydrodynamics and pore
4 structure on bacterial transport. Here, we present direct visualizations of three species of motile bacteria
5 under variable flow rates and porosities. We find that at higher flow rates, motility is less critical to the
6 transport of bacteria, as motion is controlled by hydrodynamic advection, making it difficult for bacteria to
7 move across streamlines. We show that this lack of motion across streamlines results in increased velocity
8 autocorrelation and bacterial spreading in the direction of flow. Furthermore, we find that bacteria with
9 different motility types are impacted by advection-dominated transport to different extents. At low flow
10 rates, the transport of bacteria with pili-mediated twitching motility is strongly controlled by advection,
11 whereas bacteria with flagella still display active motility. At high flow rates , we show that bacteria with
12 peritrichous flagella maintain their motility characteristics to a greater degree than bacteria with pili or
13 monotrichous flagella. We also present a detailed comparison of simulated flow fields with the experimental
14 net speeds of bacterial transport. The analysis reveals that interactions between hydrodynamics, motility,
15 and porous media geometry lead to oversampling of medium-velocity regions of a pore network by both
16 twitching and swimming bacteria. The study presents new perspectives on how different types of motile
17 bacteria are transported and dispersed in porous media aided by strength of differentially advecting fluid.

18

19 **1. Introduction**

20 Motile bacteria often live in dynamic flow environments, and their migration involves complex self-
21 propulsion strategies that are relevant to human health and ecology [1–3]. Navigating confined spaces of a
22 pore network, motile bacteria employ diverse movement modalities (e.g., turn angles, run-and-tumble, or
23 run-and-flick) that characterize their migration [4–7]. In porous media, the degree of confinement (i.e.,
24 porosity) and speed of the fluid flow strongly affect bacterial migration and modulate their interactions with
25 the surrounding environment. This, in turn, has a broad range of effects on bacteria, such as altering their
26 movement [8], behavior [9], resource acquisition [10], and signaling [11], thereby influencing their
27 metabolic functions, spatial distribution, and diversity. Spatial variations in flow velocities and the related
28 changes in shear add another level of complexity to the transport of bacteria. Transverse movement of
29 bacteria from low-shear to high-shear regions located near surfaces has been shown to result in the
30 accumulation of cells in low-velocity regions [12, 13]. This phenomenon, termed shear trapping, has been
31 identified as one major mechanism that drives initial colonization of curved surfaces and microfluidic pore
32 channels [14–16], leading to the formation of suspended biofilm structures [17, 18]. While these
33 observations have led to improvements in our understanding of bacterial transport in idealized systems,
34 there are significant gaps in our ability to quantify and predict transport behavior under complex conditions,
35 such as in pore networks designed to produce the hydrodynamics of natural porous media. Understanding
36 the motile behavior of bacteria in confined environments, in which they search for available physical space
37 and move in response to fluid flow, has implications for a wide range of applications, such as
38 bioremediation, biofilm formation, and anticancer drug delivery [19–21].

39 Here, we report direct bacterial transport visualizations, at single-cell resolution, of three different species
40 of motile bacteria under variable flow conditions in a quasi-2D porous media with different levels of pore

41 confinement. Our work focuses on investigating *Acidovorax* strain JHL-9 [22], *Geobacter sulfurreducens*
42 [23], and *Paenibacillus* strain 300A [24] due to their common attribute of metal-reducing capabilities. By
43 studying these specific microorganisms, our research findings are especially relevant to bioremediation and
44 biogeochemical cycling in terrestrial environments [25-27]. Furthermore, our selection of these species is
45 based on their distinct modes of motility. Using their pili to attach to surfaces and pull themselves towards
46 new locations [28], *Geobacter sulfurreducens* exhibit twitching motility [29]. *Paenibacillus* 300A exhibited
47 swimming motility, presumably driven by peritrichous flagella [30]. *Acidovorax* JLH-9 [22] exhibited
48 twitching motility, consistent with genomic analysis of the strain, though transmission electron microscopy
49 (TEM) images of the strain suggest the presence of polar/monotrichous flagella, indicating the possibility
50 of swimming motility as well. Swimmers generally move much faster than twitchers [28, 31-33], providing
51 a reasonable basis in this study to compare the two different motility types at different flow rates.

52 We find that regardless of the motility type, as flow rates increase, individual cells experience difficulty in
53 moving across streamlines, resulting in weaker coupling between bacterial motility and their overall
54 transport characteristics. We show that as flow speed increases, bacteria disperse faster in the direction of
55 flow, due to a lower likelihood of motion across streamlines and an increase in longitudinal displacement
56 driven by differentially advecting fluid. In other words, the distance between individual cells grows at a
57 fast rate since cells are less likely to make transverse movements (i.e., displacements across streamlines),
58 and are more likely to move longitudinally at velocities spanning a wide range of values due to the parabolic
59 nature of laminar flow profiles. Furthermore, we show that the motility of *Paenibacillus* is less impacted
60 by flows in porous media than the motilities of *Geobacter* and *Acidovorax* are, highlighting the strength of
61 peritrichous flagella-driven motility. Additionally, we provide evidence that motile bacteria tend to
62 oversample medium-velocity zones in porous media for the conditions tested in our experiments. This work
63 thus provides an improved picture of the transport of motile bacteria in confined porous media under
64 variable flow conditions, especially in relation to the impact of flow on different motility types, with
65 implications for several applications where a mechanistic understanding of pore-scale transport and
66 upscaling of bacterial transport is desired.

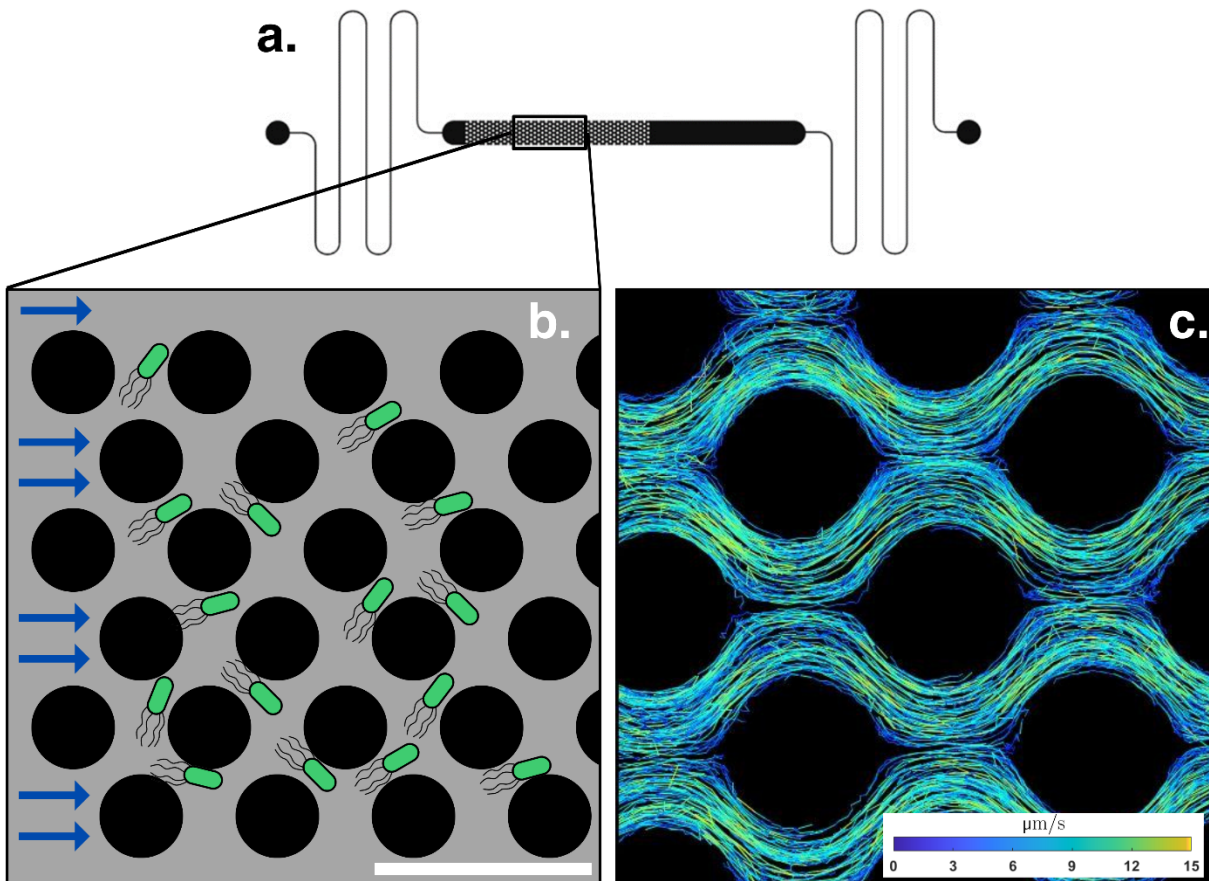
67

68 **2. Materials and Methods**

69 **2.1 Bacterial Transport in Microfluidic Devices**

70 To investigate the impacts of porosity, flow rate, and motility on bacterial transport, we recorded high-
71 resolution videos of three species of bacteria swimming in microfluidic devices [2,000 μm width \times 20 μm
72 height ($w \times h$)] at flow rates of 0 $\mu\text{L}/\text{h}$ (no flow), 1 $\mu\text{L}/\text{h}$ and 5 $\mu\text{L}/\text{h}$. The chosen flow rates allow for
73 comparative analyses of bacterial transport when the magnitude of flow speeds and bacterial motility speeds
74 are of a similar order. The micromodels were made from polydimethylsiloxane (PDMS) and contained
75 staggered pillar arrays of different grain diameters and pore lengths, resulting in either low porosity ($\phi =$
76 0.42) or high porosity ($\phi = 0.60$) micromodels. The mean fluid speeds (v_m) determined from flow rate
77 (Q), cross-sectional area (A), and porosity (ϕ) as $v_m = Q/A\phi$, in the low porosity geometries were 16.5
78 $\mu\text{m}/\text{s}$ and 82.7 $\mu\text{m}/\text{s}$, and the mean fluid speeds in the high porosity geometries were 11.6 $\mu\text{m}/\text{s}$ and 57.9
79 $\mu\text{m}/\text{s}$, for the low and high flow rates, respectively. After recording the videos, we used TrackMate [34] to
80 track, extract, and reconstruct the trajectories of individual cells (Fig. 1). Careful examination of the no-

81 flow experiment videos showed a minor drift in fluid from one end of the micromodel towards the other
82 possibly occurring due to small pressure aberrations at the inlet or outlet ports, or due to small



83
84 **Figure 1.** Experimental setup used to analyze bacterial transport in microfluidic devices. (a) A sketch of the full
85 micromodel from [35], which used the same basic micromodel schematic as our experiments. The black dots represent
86 the inlet and outlet, the black section represents an unobstructed part of the micromodel, and the gray section represents
87 the part of the micromodel with cylinders. (b) Depiction of bacteria flowing (from left to right) through a section of
88 the high porosity ($\phi = 0.60$) micromodel. The gray space represents the channels that fluid and bacteria travel
89 through, and the black circles represent the cylinders (also referred to as “grains”). The scale bar represents 120 μm .
90 Bacteria are not drawn to scale. (c) Bacterial trajectories for *Acidovorax* obtained in 5-minute interval over the course
91 of the experiment in the high porosity micromodel at a flow rate of 1 $\mu\text{L}/\text{h}$. The colormap represents net speed of
92 bacteria, with warm colors representing high speeds and cool colors representing low speeds.

93
94 axial tilt. To account for this observation in our data, we calculated the background flow (drift speed) as
95 $v_d = \frac{1}{k} \sum_0^k \frac{d}{dt} (r_{cm})$, where r_{cm} is the center of mass (x and y positions) of all bacteria in a frame, and k is
96 the number of frames (in our case, $k = 30$). To include the greatest number of possible trajectories for this
97 calculation, we reset the starting point of all trajectories to $t = 0$. We calculated mean drift speeds for
98 *Acidovorax* (0.3 $\mu\text{m}/\text{s}$), *Geobacter* (1.1 $\mu\text{m}/\text{s}$) and *Paenibacillus* (0.5 $\mu\text{m}/\text{s}$) separately.

99 Transport characteristics of bacteria were quantified using net speeds $|v_n| = \frac{\sqrt{(x_{t+1}-x_t)^2 + (y_{t+1}-y_t)^2}}{\Delta t}$, turn
100 angles $\alpha_t = \tan^{-1}\left(\frac{y_{t+2}-y_{t+1}}{x_{t+2}-x_{t+1}}\right) - \tan^{-1}\left(\frac{y_{t+1}-y_t}{x_{t+1}-x_t}\right)$, mean square displacement $MSD(t) = \frac{1}{N} \sum_{i=1}^N |r_i(t) - r_i(0)|^2$,
101 velocity autocorrelations $C_v(\tau) = \langle |v_n|(t + \tau) \cdot v(t) \rangle$, effective dispersion coefficients $D^e(t) = \frac{1}{w\phi} \int_0^w dy' D^e(t, y')$, and bivariate angle-speed probability density contours. Here x_t and y_t are individual
102 bacteria positions at time t , N is the total number of tracked cells, r_i is the displacement for bacterium i ,
103 and $|v_n|$ is the magnitude of the net velocity (i.e., speed) of the bacteria. The scripts used to calculate all
104 statistics can be found in Supplementary Methods 2. Note that the net speeds are the speed of the bacteria
105 determined through particle tracking. Since bacteria are displaced through the porous media both due to
106 their own motility and the advection imparted by the background flow, the net speed obtained via particle
107 tracking measures the combined effect of these two drivers.

109 **2.2 Micromodel Construction**

110 Micromodels for three porous geometries were constructed from PDMS using staggered arrays of grains to
111 represent porous media (see Fig. 1). The three geometries used in this experiment were (1) arrays with a
112 grain diameter (GD) of 80 μm and a pore throat length (PL) - minimum space between grains - of 20 μm
113 ($\phi = 0.42$), (2) arrays with a GD of 40 μm and a PL of 20 μm ($\phi = 0.6$), and (3) arrays with a GD of 40
114 μm and a PL of 10 μm ($\phi = 0.42$). The micromodel dimensions were 2 mm in the transverse direction, 17
115 mm in the longitudinal direction (for the porous section), and 20 μm in the vertical direction. We chose a
116 depth of 20 μm as we found that a larger depth causes bacteria to move in and out of the focal plane of our
117 camera too often.

118 **2.3 Bacteria Culture**

119 Bacterial strains *Acidovorax* JHL-9 and *Paenibacillus* 300A were grown in liquid culture aerobically at 30
120 $^{\circ}\text{C}$ on dextrose-free Trypticase Soy Broth (TSB). At late-log to stationary phase, cultures were diluted to
121 an optical density at 600 nm (OD600) of $\sim 0.1 - 0.15$ and injected into the micromodel devices described
122 above. *Geobacter sulfurreducens* was grown anaerobically (80:20 N₂:CO₂), in glass serum bottles or
123 headspace vials, crimp-sealed with butyl-rubbers stoppers, on Freshwater Medium [36] with 50 mM sodium
124 fumarate as electron acceptor in place of ferric citrate [37]. Stationary-phase *G. sulfurreducens* cells were
125 injected, without dilution, into micromodel devices that had been de-oxygenated overnight in an H₂-free
126 anoxic chamber (MBraun, O₂ < 10 ppm, 100% N₂). De-oxygenated micromodels were then removed from
127 the anoxic chamber using an anaerobic jar and were kept in the anaerobic jar until immediately before use.
128 *G. sulfurreducens* cells were removed from the serum bottle or headspace vial with a degassed (80:20
129 N₂:CO₂) 1-cc syringe and 22-gauge needle and immediately injected into the degassed micromodel.

130 **2.4 Video Acquisition**

131 All videos were collected with a confocal imaging technique on a Nikon Eclipse Ti2-U inverted microscope
132 equipped with a digital CMOS camera Hamamatsu Orca-Flash 4.0 controlled by NIS Elements imaging
133 software. The sensor pixel size was 6.5 $\mu\text{m} \times 6.5 \mu\text{m}$, and each recorded frame had a size of 2048 pixels x
134 2048 pixels. For videos at 10x magnification, the recorded domain size was 2048 x 6.5/10 = 1331.2 $\mu\text{m} \times$
135 1331.2 μm , and for videos at 20x magnification the video domain was 665.6 $\mu\text{m} \times 665.6 \mu\text{m}$. Videos were

136 recorded for 5 minutes at a variable frame rate of about 10 frames per second (between 8 and 12 frames per
137 second).

138 **2.5 Image Preprocessing**

139 The raw videos were preprocessed with background subtraction with a lag method specifically developed
140 in-house for these experiments. To capture trajectories of bacteria that may not move between two
141 successive frames, the subtracted background must be more than a few frames back in time. Standard
142 practice in background subtraction for such cases is to use the initial frame, or the mean frame, as a
143 background for the rest of the video, but this was not possible in our case due to variability in image
144 brightness throughout the video. To get around these problems, we used the 5th previous frame to perform
145 background subtraction. In other words, to subtract the background of frame 6, we calculated frame 6 minus
146 frame 1. Thus, any bacteria that moved a little over the course of 5 frames could still be identified during
147 particle tracking.

148 **2.6 Particle Tracking**

149 After background subtraction, the foreground was then loaded into ImageJ and particle tracking was
150 performed with the plugin TrackMate. For feature detection the Laplacian of Gaussian (LoG) detector was
151 used, and to link the features the Linear Assignment Problem (LAP) tracker was used. A sample output of
152 trajectories from TrackMate is given in the Supplementary Data.

153 **2.7 Flow Field Simulations**

154 We used flow field simulations to understand what parts of the flow field bacteria are likely to oversample.
155 The experimental geometry was initially digitized in Blender then refined in OpenFOAM to produce a
156 regular grid consisting of 2400 x 2400 x 72 voxels with a resolution of $\Delta x = \Delta y = .2773 \mu\text{m}$, $\Delta z =$
157 $.2778 \mu\text{m}$. The flow fields of the digitized geometries were obtained by solving the incompressible
158 Newtonian flow governed by the Navier-Stokes equations using SimpleFoam. The steady-state solver
159 belongs to the OpenFOAM package that uses semi-implicit methods for pressure linked equations
160 algorithms. Constant flow rate at specific experimental values of 1 and 5 $\mu\text{L/h}$ ($Q = 2.78 \times$
161 $10^{-13} \text{m}^3 \text{s}^{-1}$ or $Q = 1.39 \times 10^{-12} \text{m}^3 \text{s}^{-1}$) and constant pressure $P = 0 \text{ kg m}^{-1} \text{s}^{-2}$ were imposed at the
162 inlet and outlet of the domain, respectively. No-slip conditions were implemented at the fluid-solid
163 interface. We used a kinematic viscosity ν of 1.14e-6 for the fluid (TSB), given a calculated ratio of
164 $\nu_{\text{TSB}}/\nu_{\text{water}}$ of 1.14 [38]. A sample case folder for the simulation, as well as the commands used to run it
165 on a local machine, can be found in Supplementary Methods 1.

166

167 **3. Results**

168 **3.1 Advection-Dominated Transport Dynamics**

169 Advection-dominated transport is a regime of transport wherein the variable shear forces within pore
170 spaces, and dominance of flow speeds over motility speeds, restrict the ability of bacteria to move across
171 streamlines, thus guiding their motion primarily along streamlines at differential velocities. Advection-
172 dominated transport can be defined through hydrodynamic criteria such as $Pe \gg 1$ [39], or through
173 observations of bacteria such as weak coupling between motility and biofilm formation patterns [40]. This

174 type of transport has also been previously reported for bacteria in porous media flows [41]. Specifically, it
175 has been shown that cell rotation caused by shear forces results in decreased transverse dispersion and
176 increased lateral dispersion. Here, we provide additional relevant statistical information to characterize
177 advection-dominated transport for three different types of motile bacteria. In the following, we characterize
178 transport dynamics through the MSD, turn angle distribution, $C_v(\tau)$, and $D^e(t)$. We use these statistics to
179 develop a robust understanding of transport driven by differential advection, movement across streamlines,
180 velocity decorrelation, and spreading [42, 43].

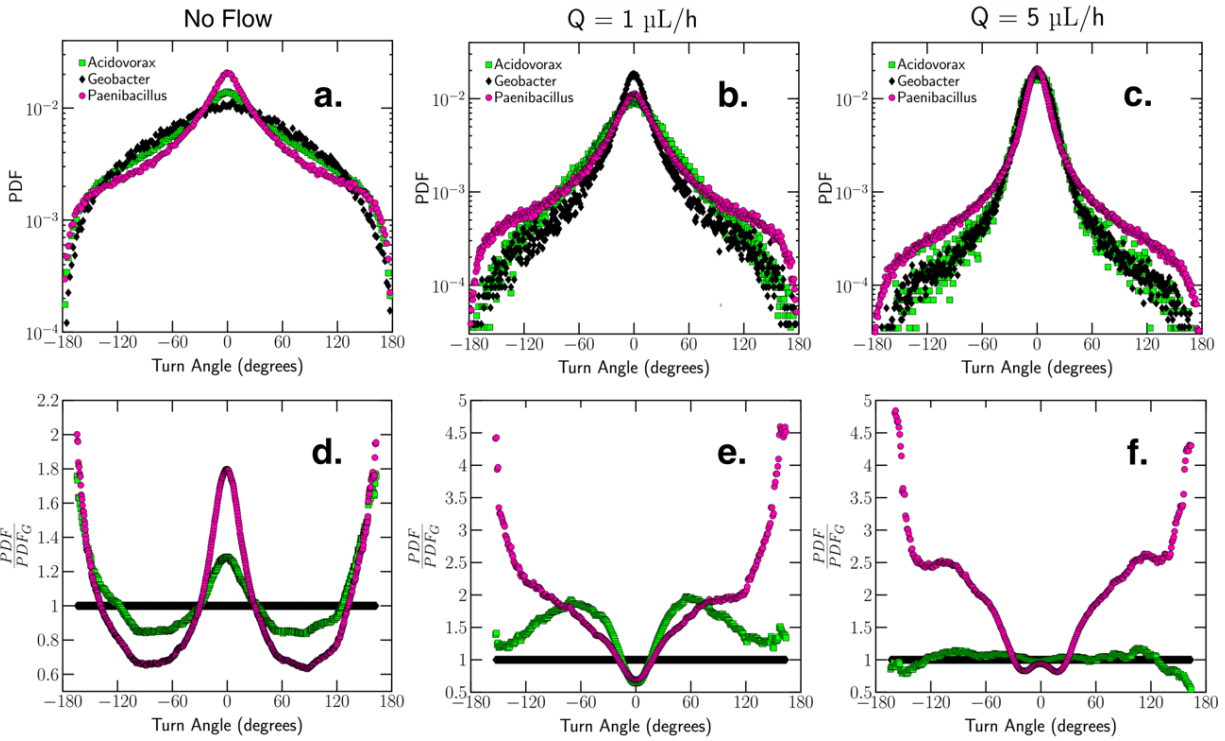
181 **3.1.1 Turn Angle Analysis Reveals Variations in Bacterial Motility**

182 To understand the motility of each species of bacteria, we primarily use turn angle distributions. It should
183 be noted here that turn angles as defined in this paper are not the same as traditionally reported turn angles
184 that reflect the body orientation during bacterial run and tumbles [44]. Because the bacterial speeds did not
185 greatly exceed the background flow speed and our experiments were performed at a relatively low frame
186 rate, we use our definition of the turn angle to capture the relative change in the trajectory of advected cells
187 between successive video frames.

188 For no-flow conditions, *Paenibacillus* (peritrichous flagella-based motility) show a high probability of low
189 or very high turn angles (Fig 2a). Low turn angles ($\alpha > -30^\circ$ or $\alpha < 30^\circ$) represent persistent forward
190 motion (i.e., long run times), and high angle turns represent reversals in direction (i.e., tumbling). Although
191 not a necessary condition, a high probability of low turn angles implies a high probability of runs, and a
192 high probability of medium to high turn angles implies a high probability of tumbling. Twitching bacteria
193 have a relatively low probability of low and high turn angles because their motion is generally more random
194 and is subject to slight changes in hydrodynamics.

195 To identify the differences in motility for each species more effectively, we also report the ratio of the turn
196 angle PDF for each species to the turn angle PDF for *Geobacter* (Figs. 2d-2f). Essentially, *Geobacter*
197 represents our twitching baseline, as their speed distributions (Supplementary Figure 1) and mean speed
198 (about 2.6 $\mu\text{m/s}$ after subtracting average drift) are generally in agreement with previously reported
199 twitching speeds of various bacteria [28, 31-33]. Thus, the PDFs of *Acidovorax* and *Paenibacillus* turn
200 angles show the relative departure from a typical twitcher (Fig. 2d). The PDF ratio for *Paenibacillus* shows
201 exactly what we expect from a swimmer – high probability of low turn angles (persistent forward motion),
202 low probability of medium turn angles (random motion), and high probability of high turn angles (direction
203 reversal). Intriguingly, the genome of *Acidovorax* JHL-9 (see data availability) contains numerous genes
204 related to twitching motility but not a complement of genes related to flagella-mediated motility. However,
205 as previously discussed, wet mount TEM images of strain JHL-9 (Supplementary Figure 2) suggest the
206 presence of polar flagella. Furthermore, the speed (Supplementary Figure 1) and turn angle ratio (Fig. 2d)
207 distributions of our no flow experiments indicate that *Acidovorax* behaves much more like *Paenibacillus*
208 than *Geobacter*. Specifically, we are not aware of any twitching species that has been shown to have max
209 speeds as high as 100 $\mu\text{m/s}$, and the turn angle PDF ratios for *Acidovorax* are very similar to those of
210 *Paenibacillus*, so it is highly unlikely that *Acidovorax* only exhibit twitching motility.

211



212

213 **Figure 2.** Turn angle PDFs for all three species in the low porosity geometry (grain diameter = 80 μm , pore length =
214 20 μm). (a) Turn angle PDF at flow rate of 1 $\mu\text{L}/\text{h}$. (b) Turn angle PDF at flow rate of 5 $\mu\text{L}/\text{h}$. (c) Turn angle PDF
215 ratio at a flow rate of 1 $\mu\text{L}/\text{h}$. (d) Turn angle PDF ratio at a flow rate of 1 $\mu\text{L}/\text{h}$. Turn angle PDF ratios are calculated
216 as the PDF/PDFG, where PDFG represents the PDF of Geobacter. We choose to make the ratios relative to *Geobacter*,
217 because they move much less (in terms of average no-flow displacement per frame) than the other bacteria.
218 Convergence of the shape of the turn angle distribution and clustering of turn angles around 0° at 5 $\mu\text{L}/\text{h}$ provide
219 evidence of advection-dominated transport. Furthermore, turn angle ratios show that both *Acidovorax* and
220 *Paenibacillus* move around and change streamlines at 1 $\mu\text{L}/\text{h}$, but only *Paenibacillus* remain active at 5 $\mu\text{L}/\text{h}$.

221

222 Compared to the case of our no-flow experiments, the interpretation of our turn angle statistics in the
223 presence of flow is slightly more complicated. We posit that in a viscous steady-state flow, non-motile
224 bacteria would behave as inert particles transported by advection only, thus moving along streamlines of
225 the pore-scale flow field, which would result in small turn angles between successive motion steps. In other
226 words, in the case of flow, persistent forward motion yields a high probability of low turn angle
227 distributions. However, motile bacteria don't only move forward. They can move across streamlines, move
228 in the reverse direction, and explore the pore space under flow conditions, and as a result, large turn angles
229 should be expected for highly active self-propelled bacteria [45-50].

230 We find that *Paenibacillus* have a higher probability of large turns ($\alpha < -90^\circ$ or $\alpha > 90^\circ$) than the other
231 two species at a flow rate of 1 $\mu\text{L}/\text{h}$, while at 5 $\mu\text{L}/\text{h}$ this difference is even more noticeable (Figs. 2b and
232 2c). Looking at the turn angle PDF ratios (Fig. 2e), we see that at 1 $\mu\text{L}/\text{h}$ *Paenibacillus* and *Acidovorax* have
233 similar distributions for low to medium turn angles, but *Paenibacillus* has a much higher probability of
234 large turn angles, indicating a greater potential for direction reversal than the other bacteria. At 5 $\mu\text{L}/\text{h}$ (Fig.

235 2f) the similarities between *Paenibacillus* and *Acidovorax* completely disappear, and the turn angle PDFs
236 for *Acidovorax* and *Geobacter* essentially converge. This implies that at high flow speeds, *Paenibacillus*,
237 with its peritrichous flagella, are either able to tumble more, or run faster, than *Acidovorax* or *Geobacter*.
238 Since the no-flow speed PDFs show that *Acidovorax* and *Paenibacillus* have similar max speeds, and
239 monotrichous and amphitrichous bacteria have generally been shown to be capable of higher speeds than
240 peritrichous bacteria [32, 51], it does not seem likely that the difference in motility between *Acidovorax*
241 and *Paenibacillus* at high speed is due to run speeds. Thus, our results imply that at high flow rates
242 *Acidovorax* are unable to tumble, but *Paenibacillus* can. This is supported by research showing that
243 increasing numbers of flagella have been shown to increase the probability of tumbling [52]. However, we
244 should also note that differences in the flagellar architecture are not the only possible explanations for
245 differences in the turn angle distributions. Two other possible explanations for this include reorientation
246 strategies, which may impact their preference to run or tumble [53], and size-related dynamics, which have
247 been shown to influence the appearance of hydrodynamic impacts on bacterial motility [54]. Regardless of
248 the exact cause, our results do show that *Paenibacillus* can maintain swimming-like behavior at higher flow
249 rates. *Acidovorax*, on the other hand, act like swimmers at low or no flow, and twitchers at high flow. In
250 other words, advection-dominated transport, which makes swimmers behave like twitchers, occurs at a
251 lower flow rate for *Acidovorax* than for *Paenibacillus*.

252 **3.1.2 Effects of Advection-Dominated Transport on Spreading**

253 Figure 3 confirms additional evidence of advection-dominated transport via the computed MSD. Here, we
254 introduce the term “differential advection” to describe the MSD results, stemming from the bacteria’s mixed
255 super-diffusive motions influenced by streamline shifts, trapping, and pore space exploration. This term
256 aptly captures the relationship between velocity decorrelation events and bacterial advection and offers a
257 nuanced description of the transport dynamics. As the flow rate increases, simple advection increases, as
258 bacteria will, on average, have a larger range of displacements at higher flow rates due to the magnitudes
259 of velocities it can sample within the laminar profile of porous media flow [15]. In addition, advection-
260 dominated transport results in smaller turn angles at the high flow rate, which implies less streamline
261 changing. This results in higher values of the MSD driven by increased differential advection as bacteria
262 are transported by a range of velocities produced by converging and diverging streamlines within the pore
263 network.

264 Complementing the increased differential advection, as the flow rate increases, the MSDs of all species of
265 bacteria in the low porosity geometry (Figs. 3d and 3e) show signs of convergence (both in slope and
266 magnitude), likely driven by decorrelation of cell swimming as bacteria encounter pore structures [49].
267 Essentially, advection-dominated transport is thus revealed by the convergence (between different species
268 of bacteria) of both turn angle and MSD, and a shift toward greater differential advection. In contrast, with
269 the high porosity geometry, we observe less evidence of MSD convergence, which indicates that the flow
270 speeds are not high enough to suppress bacterial motility, leading to a reduction in differential advection as
271 shown by lower MSD values (Figs. 3b and 3c). We also find that for a fixed porosity and flow rate,
272 *Geobacter* and *Acidovorax* always advect more than *Paenibacillus*, further supporting the idea that
273 peritrichous swimmers are differentially advected to a lesser degree than twitchers or polar swimmers.

274

275

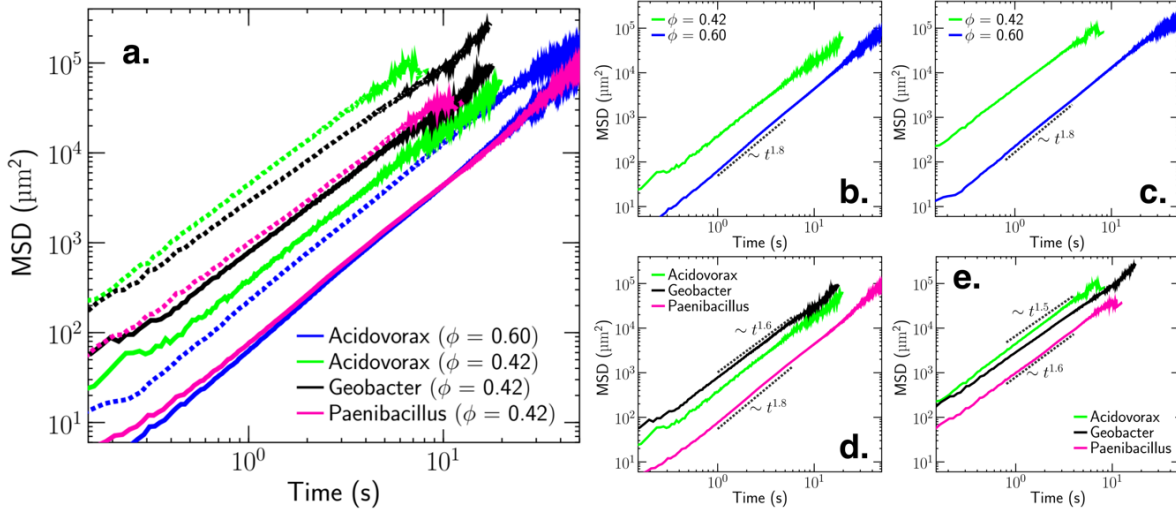


Figure 3. Mean square displacements (MSDs) at different porosities and flow rates for three different species of bacteria. **(a)** All MSDs from relevant experiments (3 species, 2 porosities, 2 flow rates). The 1 $\mu\text{L}/\text{h}$ results are shown as solid lines and the 5 $\mu\text{L}/\text{h}$ results are shown as dotted lines. This figure is useful for comparisons with Fig. 6. **(b)** MSDs for *Acidovorax* for $\phi = 0.60$ and $\phi = 0.42$ at a flow rate of 1 $\mu\text{L}/\text{h}$ (mean fluid speed of 11.6 $\mu\text{m}/\text{s}$ and 16.5 $\mu\text{m}/\text{s}$ respectively). **(c)** MSDs for *Acidovorax* for $\phi = 0.60$ and $\phi = 0.42$ at a flow rate of 5 $\mu\text{L}/\text{h}$ (mean fluid speeds of 57.9 $\mu\text{m}/\text{s}$ and 82.7 $\mu\text{m}/\text{s}$ respectively). **(d)** MSDs for all species for $\phi = 0.42$ at a flow rate of 1 $\mu\text{L}/\text{h}$. **(e)** MSDs for all species for $\phi = 0.42$ at a flow rate of 5 $\mu\text{L}/\text{h}$. These figures show an increase in the impact of differential advection (value of the MSD) for motile bacteria as the flow rate increases. The rapid increase in MSD driven by differential advection, along with convergence of the MSDs in the low porosity geometry at 5 $\mu\text{L}/\text{h}$, provide evidence of advection-dominated transport. At both flow speeds, *Paenibacillus* show lower values of MSD than *Geobacter* or *Acidovorax*, indicating a stronger resistance to advection-dominated transport. All low porosity results in this figure are from the grain diameter = 80 μm , pore length = 20 μm geometry.

To further understand spreading in our experiments, we calculated the effective dispersion coefficient, D^e , based on the average spatial variance of the bacteria distribution evolving from a pointlike injection, that is, the transport Green function as defined in [55, 56]. At 1 $\mu\text{L}/\text{h}$, D^e represents spreading in both the longitudinal and transverse directions for *Paenibacillus* and *Acidovorax*, but only in the longitudinal direction for *Geobacter* owing to its considerably lower twitching speed than the mean fluid speed. At 5 $\mu\text{L}/\text{h}$, D^e primarily represents longitudinal dispersion for all species. Our results show that when the flow rate increases from 1 $\mu\text{L}/\text{h}$ to 5 $\mu\text{L}/\text{h}$, D^e increases the most for *Geobacter*, and the least for *Paenibacillus* (Table 1). Because *Paenibacillus* are able to maintain some form of motility at 5 $\mu\text{L}/\text{h}$, and as a result are still able to change streamlines and explore the pore space, differential advection has less of an impact on their dispersion than it does for the dispersion of *Geobacter* and *Acidovorax*. Overall, our observations illustrate that the bacteria that follow streamlines or explore less space in the transverse direction to the flow, advect and spread more in the direction of flow. These results complement those presented in [41], which showed that hydrodynamic gradients in a similar porous geometry reduce transverse dispersion. We further this research by showing that bacterial transport is advective-dominated for a wide variety of flow rates depending on the type of bacterial motility.

314 **Table 1.** Effective Bacterial Dispersion Coefficients D^e ($\mu\text{m}^2/\text{s}$) for all experiments. All results are for the low
 315 porosity geometry ($\phi = 0.42$). Standard deviations are calculated from the set of all D^e values calculated for each 8th
 316 of the domain (eg. $y_1 = 0: 256, y_2 = 256: 512$). As flow speed increases, *Geobacter* have the greatest increase in
 317 dispersion and *Paenibacillus* have the smallest increase in dispersion. At 5 $\mu\text{L}/\text{h}$ advection-dominated transport is
 318 apparent for *Geobacter* and *Acidovorax*, implying that differential advection results in a relative increase in dispersion.
 319 Because the motility speeds of the bacteria are less than the fluid speed at 5 $\mu\text{L}/\text{h}$, dispersion is almost entirely in the
 320 direction of flow for the 5 $\mu\text{L}/\text{h}$ experiments.

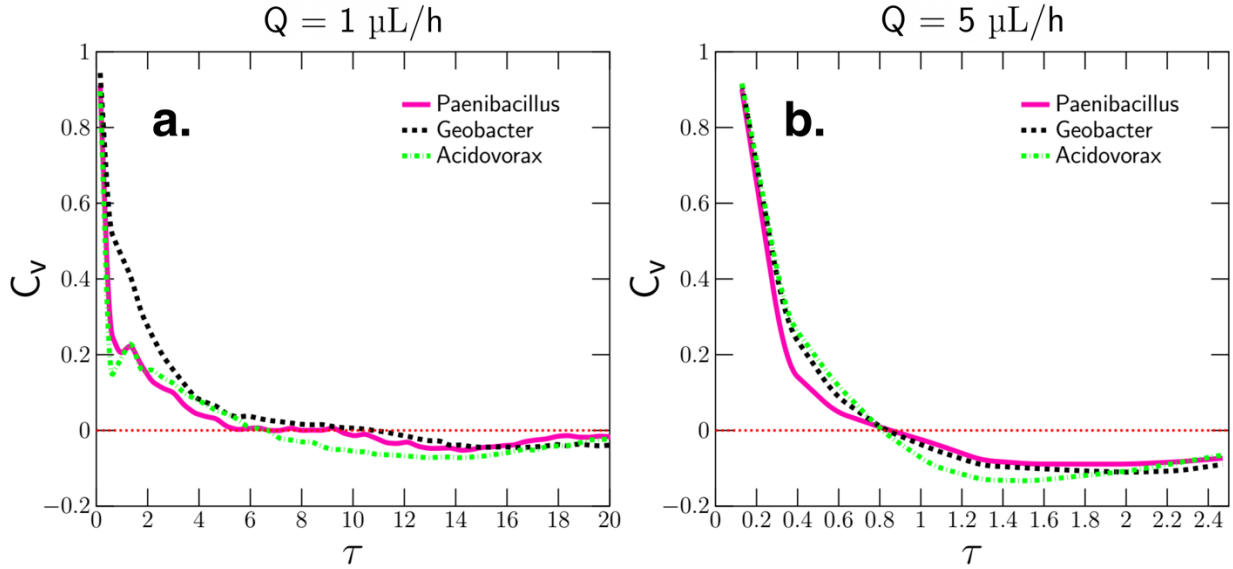
D^e	<i>Paenibacillus</i>	<i>Geobacter</i>	<i>Acidovorax</i>
1 $\mu\text{L}/\text{h}$	107 ± 46	308 ± 97	204 ± 56
5 $\mu\text{L}/\text{h}$	217 ± 43	895 ± 148	466 ± 74

321

322 3.1.3 Impact of Advection-Dominated Transport on Velocity Autocorrelation

323 We use the velocity autocorrelation function (C_v) to further provide information on advection-dominated
 324 transport. Generally, in porous media, bacteria show uncorrelation in velocities over time due to a tendency
 325 for sampling different portions of the flow field and trapping events (i.e., pore confinement, occurrence of
 326 collisions and attachment to obstacles) [6, 57]. Previous research has shown that uncorrelation of bacterial
 327 trajectories is more rapid at high flow rates [41]. Our findings both confirm these trends and present new
 328 information on how motility type impacts uncorrelation. We show that *Paenibacillus* and *Acidovorax*
 329 exhibit uncorrelation faster than *Geobacter* at 1 $\mu\text{L}/\text{h}$ (Fig. 4a), but that at 5 $\mu\text{L}/\text{h}$, all uncorrelation times
 330 are essentially the same. This suggests that at low flow rates swimmers experience larger variations in
 331 velocity over time by sampling multiple streamlines and trapping events that decorrelate subsequent
 332 velocities. However, as flow rate increases, motility type no longer has any significant impact on the
 333 probability of decorrelation events. These observations further support the presence of flagella-based
 334 swimming for *Acidovorax* at 1 $\mu\text{L}/\text{h}$. Furthermore, we show that advective-dominated transport can be
 335 observed through a convergence of C_v uncorrelation times. These trends generally agree with the
 336 observations of the MSD, D^e and turn angle distribution analysis, although the C_v is slightly less sensitive
 337 to differences in motility than the other metrics.

338



339

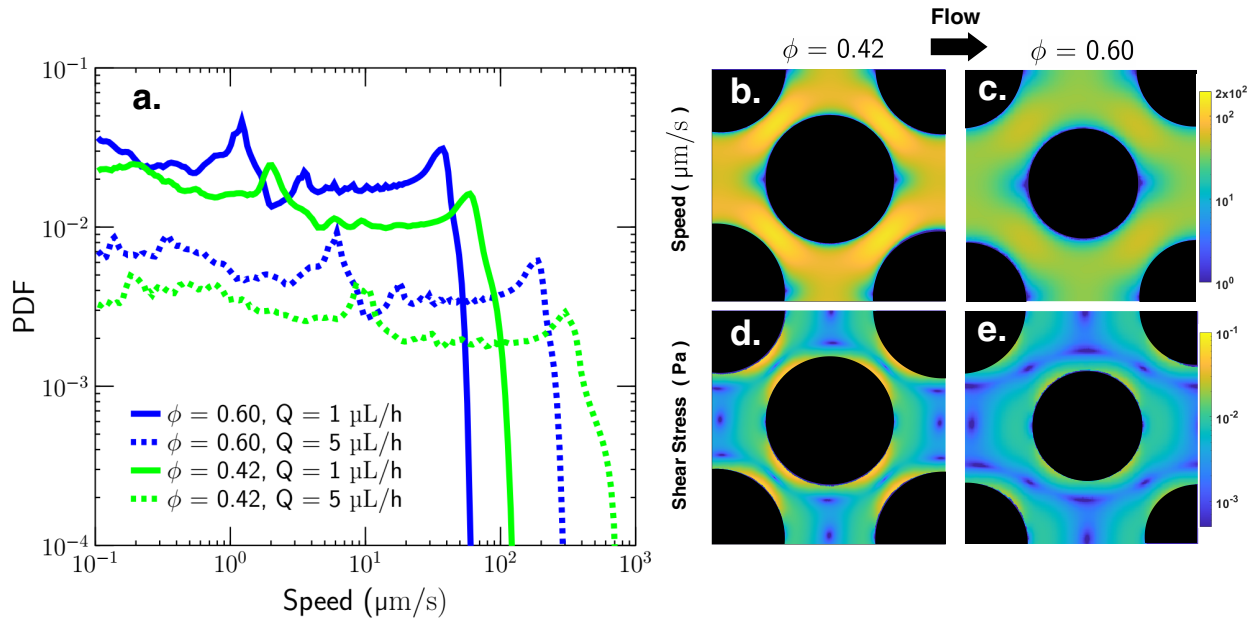
340 **Figure 4.** Velocity Autocorrelation functions (C_v) for the low porosity experiments at (a) $1 \mu\text{L}/\text{h}$ and (b) $5 \mu\text{L}/\text{h}$. The
 341 swimming species (*Paenibacillus* and *Acidovorax*) show faster decorrelation than the twitching species (*Geobacter*)
 342 at $1 \mu\text{L}/\text{h}$ since the twitching species are more likely to go with the flow. At $5 \mu\text{L}/\text{h}$ the C_v for the plots for twitching
 343 species converges, which is further evidence of advection-dominated transport.

344

345 3.2 Spatial Variations in Net Speeds

346 We digitized the experimental microfluidic geometries and simulated the steady-state viscous flow at high
 347 resolution using SimpleFoam [58, 59] to determine how bacteria under or oversample different parts of a
 348 flow field (Fig. 5). By comparing the obtained simulated distribution of fluid speeds against the
 349 experimentally derived distribution of net bacterial speeds, we can develop an understanding of the zones
 350 within a pore network that bacteria may preferentially occupy. We recognize that a more accurate
 351 comparison would use flux weighting and particle tracking to compare the simulated fluid speed PDFs with
 352 the net bacterial speed PDFs. However, given the large number of trajectories (tens of thousands for each
 353 bacteria), and the periodic nature of our flow field, we posit that the trajectories of tracked bacteria
 354 adequately sample the domain space and thus provide basis for comparison to simulated speeds.

355 We observe that regardless of flow rate, motility type, or porosity, motile bacteria in porous media tend to
 356 undersample low-speed zones and oversample medium-speed zones (relative to the Eulerian fluid speed
 357 PDF) (Fig. 6). This provides additional insight to the notion of shear trapping which suggests bacteria in a
 358 shear flow will oversample low-speed zones [60, 61]. A plausible explanation for this observed difference
 359 lies in recognizing that studies reporting shear trapping were often conducted in simpler geometries (e.g.,
 360 straight channels) [12] than periodic array of cylinders inducing converging and diverging streamlines in
 361 our study. However, an exact relationship

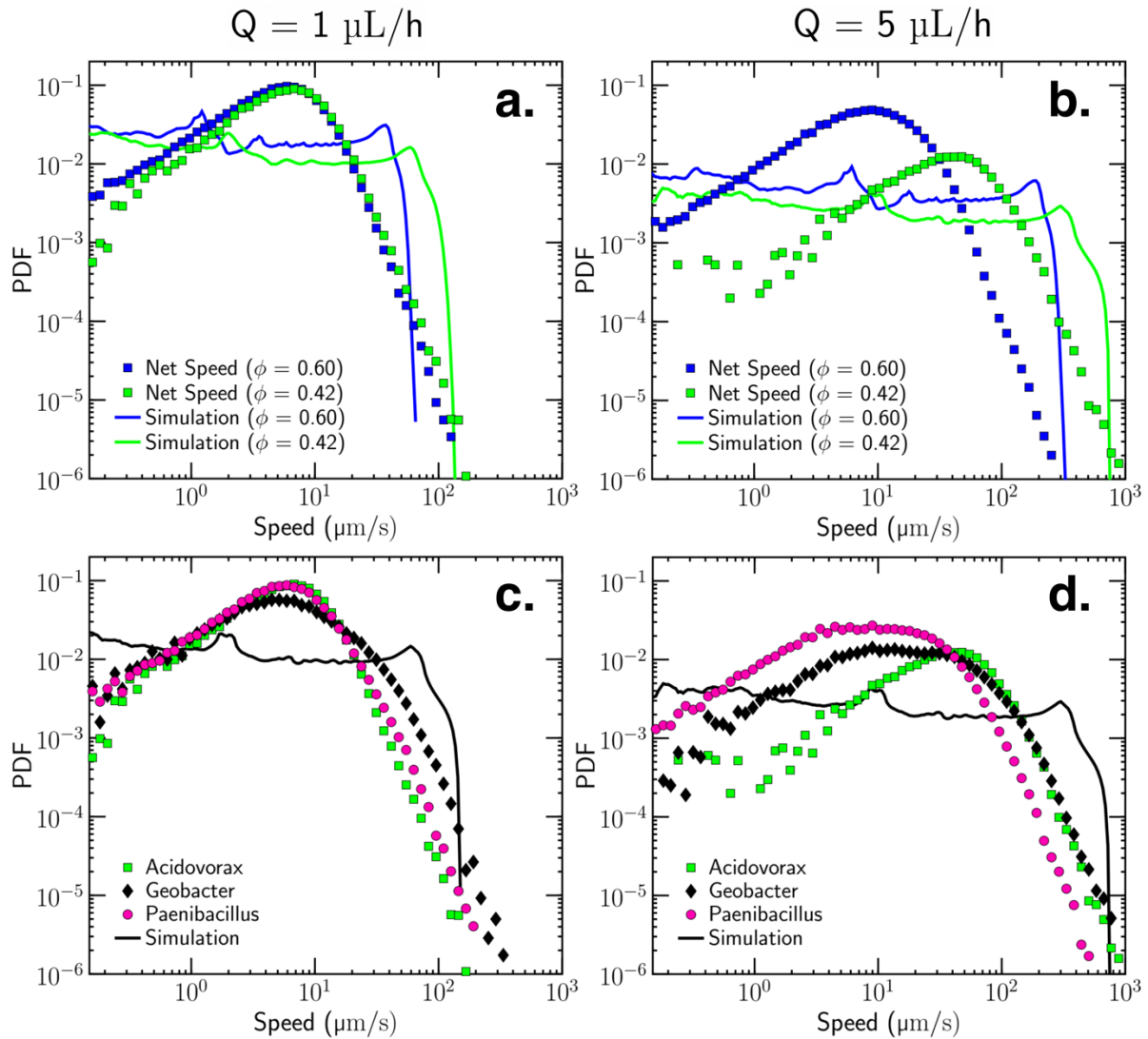


362

363 **Figure 5.** Results from the steady-state viscous flow simulations of our experimental microfluidic geometries. All low
 364 porosity results in this figure are from the grain diameter = 80 μm , pore length = 20 μm geometry. **(a)** Probability
 365 distribution functions (PDFs) of fluid speed from the simulated flow fields for each porosity and flow rate used in our
 366 experiments. **(b)** Zoomed-in velocity magnitude field for the low porosity simulation at 1 $\mu\text{L}/\text{h}$. **(c)** Zoomed-in velocity
 367 magnitude field for the high porosity simulation at 1 $\mu\text{L}/\text{h}$. **(d)** Zoomed-in shear stress magnitude field for the low
 368 porosity simulation at 1 $\mu\text{L}/\text{h}$. **(e)** Zoomed-in shear stress magnitude field for the high porosity simulation at 1 $\mu\text{L}/\text{h}$.

369

370 between hydrodynamics and the observed medium speed sampling cannot be deduced in our study because
 371 of lack of high-resolution tracking necessary to compute shear-induced lateral transport towards the walls
 372 due to Jeffrey orbits [62-64]. Another potential explanation of oversampling of medium-speed zones is that
 373 high levels of shear (closer to the walls) can prevent bacteria from bundling their flagella [65]. In this
 374 unbundled state, the bacteria act as deformable objects resulting in a stokes lift force as they approach
 375 surfaces. In addition, size exclusion and hydrodynamic chromatography have shown that the transport of
 376 microbes is dependent on size and shape [66, 67]. Size exclusion occurs because bacteria are too large to
 377 only occupy the slow speed zones around the grain [68]. Unless they are attached, bacteria will move more
 378 quickly around the grain than a solute will because part of their body is in higher speed zones. Finally,
 379 electrostatic repulsion, or the likely presence of energy barriers close to the grains, may prevent bacteria
 380 from getting too close to surfaces [16, 48, 69-72]. The wide variety of plausible explanations for of shear
 381 trapping in our study illustrate the complexities of analyzing bacterial transport in porous media.



382

383 **Figure 6.** PDFs of net speed. All low porosity results in this figure are from the grain diameter = 80 μm , pore length
384 = 20 μm geometry. **(a)** Net and simulated speed distributions for *Acidovorax* for $\phi = 0.60$ and $\phi = 0.42$ at a flow
385 rate of 1 $\mu\text{L/h}$. **(b)** Net and simulated speed distributions for *Acidovorax* for $\phi = 0.60$ and $\phi = 0.42$ and flow rate of
386 5 $\mu\text{L/h}$. **(c)** Net and simulated speeds for all species for $\phi = 0.42$ at a flow rate of 1 $\mu\text{L/h}$. **(d)** Net and simulated
387 speeds for all species for $\phi = 0.42$ at a flow rate of 5 $\mu\text{L/h}$. These figures show the net speeds of the bacteria overlaid
388 by the simulated speeds for the respective flow rate and porosity. The net speeds are represented by scatter points,
389 whereas the simulated speeds are represented by solid lines. All simulated PDFs represent the distribution of Eulerian
390 flow speeds for that geometry. These figures show the tendency for motile bacteria to oversample medium-speed
391 zones within a porous media.

392

393 In no-flow conditions, the 95th percentile of speeds for *Geobacter* is about 8.5 $\mu\text{m/s}$, for *Acidovorax* its 17
394 $\mu\text{m/s}$, and for *Paenibacillus* it's 21 $\mu\text{m/s}$. At the low flow rate of 1 $\mu\text{L/h}$ (16.5 $\mu\text{m/s}$), the swimming speeds
395 of *Acidovorax* and *Paenibacillus* can thus exceed the fluid flow speeds, but at 5 $\mu\text{L/h}$, none of the bacteria
396 we tested can consistently exceed the fluid flow speed. Thus, advection-dominated transport in its simplest

397 form is a result of flow speeds exceeding motility speeds. However, shear adds another layer of complexity
398 when considering the ability for bacteria to bundle/unbundle their flagella. Recent work has shown that at
399 a shear magnitude of about 0.26 Pa, *E. Coli* lose control over this mechanism and can't effectively swim
400 [65]. The 1 $\mu\text{L}/\text{h}$ simulations in our study do not produce shear exceeding this value (Figs. 5d and 5e), but
401 at 5 $\mu\text{L}/\text{h}$, the value of shear close to the grain is larger than this threshold value. Although a simulation of
402 threshold shear magnitudes for bundling abilities in *Paenibacillus* and *Acidovorax* was beyond the scope
403 of this paper, this inability to control motility [73] through bundling/unbundling of flagella remains a likely
404 explanation for the differences observed in the motilities of *Paenibacillus* and *Acidovorax*. It should be
405 noted that in our quasi-2D porous media, under uniform and laminar flow, there are no chemotactic or
406 thermal gradients influencing the transport. Thus, the magnitude and distribution of shear within a porous
407 media, which attains its maximum value at grain surfaces and is minimum along centerlines of a pore
408 channel, is likely the primary physical mechanism that controls bacterial transport.

409 **3.3 Turn Angle and Net Speed Dynamics**

410 We further analyze the combined influence of net speed and turn angle on the advective spreading of motile
411 bacteria using a matrix of bivariate (speed-angle) joint probability density contours (Fig. 7). The probability
412 density matrix allows us to observe general relationships between the differential advection plotted in Fig.
413 3a, and the turn angles and net speeds of the bacteria. As net speed increases, bacteria have a narrower
414 range of turn angles and, therefore, greater spreading in the longitudinal direction stems from strongly
415 advective particle motion. In the top and middle rows of Fig. 7, larger turn angles and less spreading are
416 seen from left to right. In the bottom row, there is no significant change in large-angle turns or advective
417 spreading. Thus, somewhere between the middle and bottom rows, or around a median speed of 50-100
418 $\mu\text{m}/\text{s}$, the impacts of advection-dominated transport increase to the extent that changes in fluid speed causes
419 insignificant difference in advective spreading or turn angle for bacteria of the same motility type. This
420 suppression in active dispersion in the case of strong fluid flow corroborates recent studies of transport of
421 actively moving particles in porous media [74]. In addition to providing deeper insight into the transition
422 to the advection-dominated regime, the joint probability density matrix also shows that bacteria are more
423 likely to make large turns at low speeds than at high speeds. Conversely, small-angle turns are more likely
424 to occur at high speeds than large-angle turns. When bacteria are moving with faster streamlines, their turn
425 angles are smaller as they are more likely to go with the flow. When moving with slower streamlines,
426 bacteria are more likely and more able to make large turns and cross transversely to other streamlines. This
427 provides further evidence that pore space exploration and movement across streamlines require low fluid
428 speeds and results in large turn angles.

429

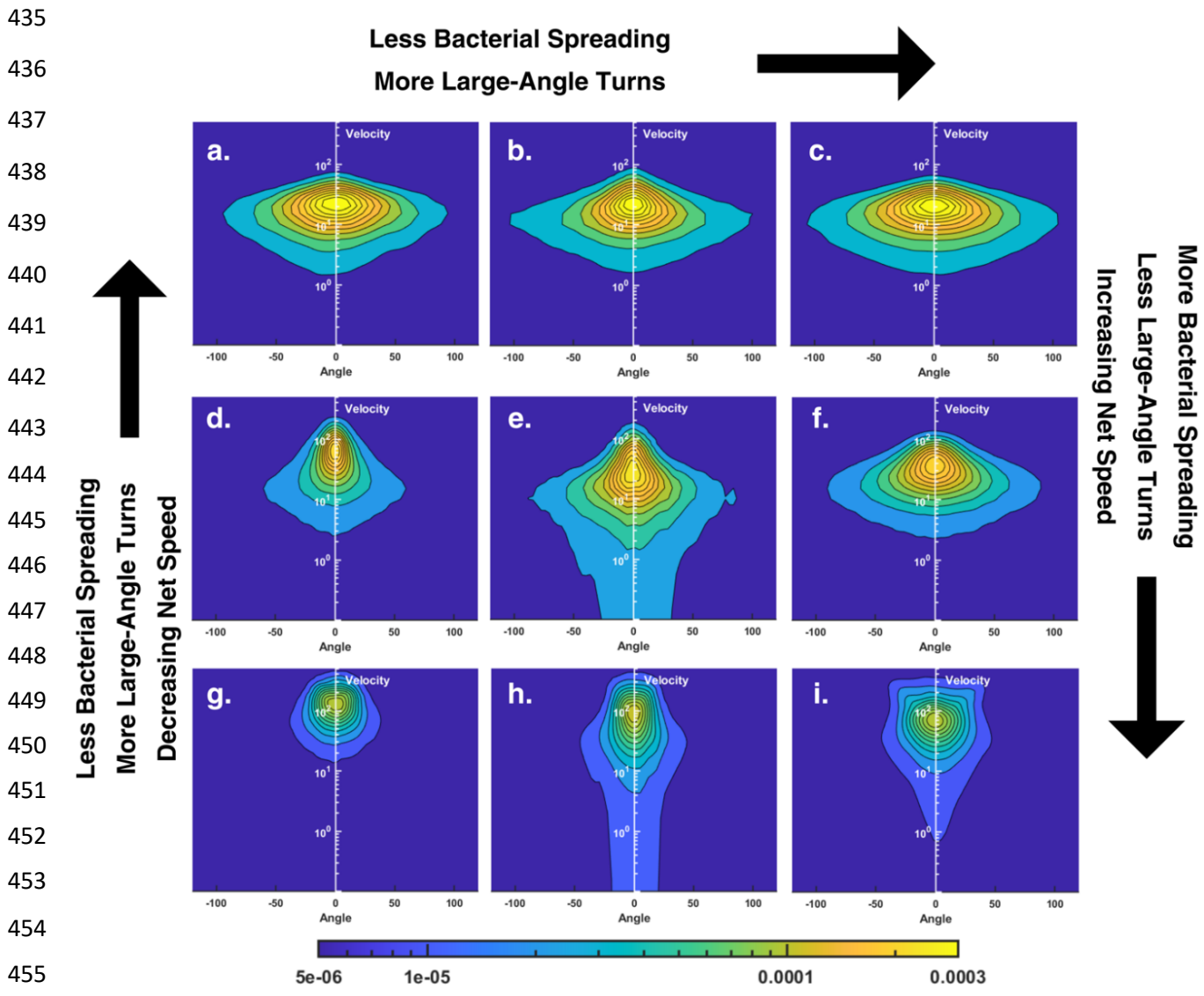
430

431

432

433

434



456
 457 **Figure 7.** Velocity-angle joint probability density matrix. (a) *Acidovorax*, $\phi = 0.42$, $1 \mu\text{L}/\text{h}$ (grain diameter = $80 \mu\text{m}$,
 458 pore length = $20 \mu\text{m}$) (b) *Paenibacillus*, $\phi = 0.42$, $1 \mu\text{L}/\text{h}$ (c) *Acidovorax*, $\phi = 0.60$, $1 \mu\text{L}/\text{h}$ (d) *Paenibacillus*, $\phi =$
 459 0.42 , $5 \mu\text{L}/\text{h}$ (e) *Geobacter*, $\phi = 0.42$, $1 \mu\text{L}/\text{h}$ (f) *Acidovorax*, $\phi = 0.60$, $5 \mu\text{L}/\text{h}$ (g) *Geobacter*, $\phi = 0.42$, $5 \mu\text{L}/\text{h}$ (h)
 460 *Acidovorax*, $\phi = 0.42$, $5 \mu\text{L}/\text{h}$ (grain diameter = $80 \mu\text{m}$, pore length = $20 \mu\text{m}$) (i) *Acidovorax*, $\phi = 0.42$, $5 \mu\text{L}/\text{h}$ (grain
 461 diameter = $40 \mu\text{m}$, pore length = $10 \mu\text{m}$). Each figure in the density matrix shows probability density contours for net
 462 speed and turn angle for a particular set of conditions. As we move across the matrix from bottom to top, we see
 463 decreased net speeds, increased large-angle turns, and less spreading. As we move from left to right across the matrix,
 464 we see a slight increase in large-angle turns and decrease in spreading, but not as much as going from bottom to top.
 465 There is no significant change in net speed moving from left to right. This figure implies that fast net speeds are
 466 required for bacteria to be in the advection-dominated regime, which results in more small-angle turns. Furthermore,
 467 past a threshold speed of about $50\text{-}100 \mu\text{m}/\text{s}$, motile bacteria are unlikely to have large-angle turns.

468

469 **4. Discussion**

470 This study primarily investigates the impact of flow rates and porosity on the variable transport of different
471 species of motile bacteria in porous media. We show that *Geobacter*, with their purely twitching-based
472 motility, are not fast enough to show any impacts of motility on their transport at low or high flow rates.
473 *Paenibacillus*, with their peritrichous flagella, exhibit strong swimming motility. Although they exhibit
474 weak motion across streamlines and exploration of pore space at high flow rates, their turn angle
475 distributions reflect a higher degree of activity. In the middle of the twitchers and swimmers are *Acidovorax*.
476 They behave like swimmers at no-flow and at a flow rate of 1 $\mu\text{L}/\text{h}$, but at 5 $\mu\text{L}/\text{h}$, they behave more like
477 twitchers. Although a deep investigation of the motility type of *Acidovorax* is beyond the scope of this
478 work, we show that differences in flagellar architecture offer a reasonable explanation for their behavior.
479 Our results and previous imaging of *Acidovorax* suggest that they have a single polar flagellum as opposed
480 to the peritrichous flagella of *Paenibacillus*. At high flow rates, it appears that peritrichous flagella are more
481 able to facilitate tumbling behavior, and thus, movement across streamlines.

482 In the advection-dominated transport regime, lack of pore space exploration and streamline changing results
483 in less transverse movement and thus leads to an overall increase in transported distance and spread in the
484 direction of flow. We show that advection-dominated transport is revealed through convergence of turn
485 angle distributions, MSDs, effective dispersion coefficients, and a clustering of turn angles around 0° . This
486 study also provides contrasting results to the notion of shear trapping wherein motile bacteria are expected
487 to oversample low-velocity regions in a shear flow. In the case of our complex porous geometry, we observe
488 bacteria oversampling medium-speed regions. When the geometry of pore channels allows for convergence
489 and divergence of streamlines in 2D space, producing hydrodynamic patterns typically found in realistic
490 porous media, wide-ranging values of shear forces emerge, leading to an interesting interplay between
491 shear, motility, and the overall bacterial transport. We discuss that this oversampling of medium speeds can
492 be a result of several different hydrodynamic or biophysical properties, and we identify shear as a likely
493 physical phenomenon underpinning our observed transport patterns.

494 Our work complements previous studies that have shown advection to dominate the transport of bacteria at
495 high flow rates, effectively erasing the differences in motile behavior between different species of bacteria
496 [12, 16, 60, 69, 75]. Our work also builds upon the body of evidence showing that there are significant
497 transport differences between swimmers and twitchers [76, 77], and that bacteria with straighter paths (non-
498 motile) spread more (in the direction of flow) than bacteria with exploratory paths (motile) at low flow
499 speeds [15]. We thus advance multiple threads of research in the field of bacterial transport. We expect the
500 results presented here to help future researchers in developing more robust experiments and models for
501 numerous applications such as bioremediation, targeted drug delivery, biofilms, biogeochemistry,
502 agriculture, infectious disease, and microbial ecology.

503 While we have tried to provide a robust analysis of bacterial transport in homogeneous porous media under
504 different flow rates, we also recognize that our study contains many limitations. The bacteria were difficult
505 to image and required large exposure times, which resulted in low frame rates and significant light scattering
506 around the grains, thus impacting the accuracy of particle tracking. Furthermore, the low frame rate
507 prevented us from analyzing bacteria through traditional run and tumble statistics. We also recognize that
508 a more expansive set of experiments would have included a wider variety of flow rates, which would allow
509 for more confidence in any trends observed between motility and flow rate. Also, although we have mainly

510 attributed the differences in transport of our three species to their differences in motility, there are other
511 phenomena, such as the impact of hydrodynamics on different cell lengths (i.e., size exclusion), and DLVO
512 and steric interactions [5], which could offer supporting explanations. Finally, we recognize that a more
513 complete study of the impacts of flow rate on the transport of different bacteria would examine the impact
514 of shear on the ability for monotrichous and peritrichous flagella to bundle/unbundle. These limitations
515 show that there is still significant work to be done to develop a mature theory of bacterial transport in porous
516 media flows.

517

518 **Data Availability**

519 Besides the raw video and trajectory data, we have provided most of the other data and scripts required to
520 replicate our findings in the supplementary materials. Raw video and trajectory data are available from the
521 corresponding author upon reasonable request. The genome for *Acidovorax* JHL-9 can be found at:
522 https://genome.jgi.doe.gov/portal/AcispJHL9_FD/AcispJHL9_FD.info.html.

523

524 **Acknowledgments**

525 This research is based upon work supported by the U. S. Department of Energy (DOE) under award number
526 DE-SC0019437. The experiments were performed on a project award
527 (<https://doi.org/10.46936/ltds.proj.2020.51218/60006749>) from the Environmental Molecular Sciences
528 Laboratory (EMSL), a DOE Office of Science User Facility sponsored by the Biological and Environmental
529 Research program, and were partially supported by the Laboratory Directed Research and Development
530 (LDRD) Program at Pacific Northwest National Laboratory. A portion of these data were produced by the
531 US Department of Energy Joint Genome Institute (<https://ror.org/04xm1d337>; operated under Contract No.
532 DE-AC02-05CH11231) in collaboration with the user community. The authors would specifically like to
533 acknowledge the micromodel fabrication help received from Dr. Hardeep Mehta at EMSL and microscopy
534 assistance from EMSL's Tom Wietsma. PNNL is a multi-program national laboratory operated for the U.S.
535 Department of Energy (DOE) by Battelle Memorial Institute under Contract No. DE-AC05-76RL0-1830.
536

537 **References**

- 538 [1] Persat, A. Nadell, C.D., Kim, M.K., Ingremeau, F., Siryaporn, A., Drescher, K., Wingreen, N.S.,
539 Bassler, B.L., Gitai, Z., & Stone, H.A. The mechanical world of bacteria, *Cell* **161**, 988-997 (2015).
- 540 [2] Yang, P. & Van Elsas, J. D. Mechanisms and ecological implications of the movement of bacteria in
541 soil. *Applied Soil Ecology* **129**, 112–120 (2018).
- 542 [3] Jalili-Firoozinezhad, S., Gazzaniga, F.S., Calamari, E.L., Camacho, D.M., Fadel, C.W., Bein, A.,
543 Swenor, B., Nestor, B., Cronce, M.J., Tovagliari, A. & Levy, O. A complex human gut microbiome cultured
544 in an anaerobic intestine-on-a-chip. *Nat Biomed Eng* **3**, 520–531 (2019).
- 545 [4] Mitchell, J. G. & Kogure, K. Bacterial motility: links to the environment and a driving force for
546 microbial physics: Bacterial motility. *FEMS Microbiology Ecology* **55**, 3–16 (2006).

- 547 [5] Tokárová, V., Sudalaiyadum Perumal, A., Nayak, M., Shum, H., Kašpar, O., Rajendran, K.,
548 Mohammadi, M., Tremblay, C., Gaffney, E.A., Martel, S. & Nicolau Jr, D.V. Patterns of bacterial motility
549 in microfluidics-confining environments. *Proc. Natl. Acad. Sci. U.S.A.* **118**, e2013925118 (2021).
- 550 [6] Perez, L. J., Bhattacharjee, T., Datta, S. S., Parashar, R. & Sund, N. L. Impact of confined geometries
551 on hopping and trapping of motile bacteria in porous media. *Phys. Rev. E* **103**, 012611 (2021).
- 552 [7] Bhattacharjee, T. & Datta, S.S. Confinement and activity regulate bacterial motion in porous media. *Soft
553 Matter*, **15**(48), pp.9920-9930 (2019).
- 554 [8] Scheidweiler, D., Miele, F., Peter, H., Battin, T. J. & De Anna, P. Trait-specific dispersal of bacteria in
555 heterogeneous porous environments: from pore to porous medium scale. *J. R. Soc. Interface*. **17**, 20200046
556 (2020).
- 557 [9] Makarchuk, S., Braz, V. C., Araújo, N. A. M., Círcic, L. & Volpe, G. Enhanced propagation of motile
558 bacteria on surfaces due to forward scattering. *Nat Commun* **10**, 4110 (2019).
- 559 [10] Perez, L. J., Parashar, R., Plymale, A. & Scheibe, T. D. Contributions of biofilm-induced flow
560 heterogeneities to solute retention and anomalous transport features in porous media. *Water Research* **209**,
561 117896 (2022).
- 562 [11] Ariel, G., Rabani, A., Benisty, S., Partridge, J.D., Harshey, R.M. & Be'Er, A. Swarming bacteria
563 migrate by Lévy Walk. *Nat Commun* **6**, 8396 (2015).
- 564 [12] Rusconi, R., Guasto, J. S. & Stocker, R. Bacterial transport suppressed by fluid shear. *Nature Phys* **10**,
565 212–217 (2014).
- 566 [13] Barry, M. T., Rusconi, R., Guasto, J. S. & Stocker, R. Shear-induced orientational dynamics and spatial
567 heterogeneity in suspensions of motile phytoplankton. *J. R. Soc. Interface*. **12**, 20150791 (2015).
- 568 [14] Yawata, Y., Nguyen, J., Stocker, R. & Rusconi, R. Microfluidic Studies of Biofilm Formation in
569 Dynamic Environments. *J Bacteriol* **198**, 2589–2595 (2016).
- 570 [15] Creppy, A., Clément, E., Douarche, C., D'Angelo, M. V. & Auradou, H. Effect of motility on the
571 transport of bacteria populations through a porous medium. *Phys. Rev. Fluids* **4**, 013102 (2019).
- 572 [16] Secchi, E., Vitale, A., Miño, G.L., Kantsler, V., Eberl, L., Rusconi, R. & Stocker, R. The effect of flow
573 on swimming bacteria controls the initial colonization of curved surfaces. *Nat Commun* **11**, 2851 (2020).
- 574 [17] Rusconi, R., Lecuyer, S., Guglielmini, L. & Stone, H. A. Laminar flow around corners triggers the
575 formation of biofilm streamers. *J. R. Soc. Interface*. **7**, 1293–1299 (2010).
- 576 [18] Rusconi, R., Lecuyer, S., Autrusson, N., Guglielmini, L. & Stone, H. A. Secondary Flow as a
577 Mechanism for the Formation of Biofilm Streamers. *Biophysical Journal* **100**, 1392–1399 (2011).
- 578 [19] Pieper, D. H. & Reineke, W. Engineering bacteria for bioremediation. *Current Opinion in
579 Biotechnology* **11**, 262–270 (2000).
- 580 [20] Ginn, T.R., Wood, B.D., Nelson, K.E., Scheibe, T.D., Murphy, E.M. & Clement, T.P. Processes in
581 microbial transport in the natural subsurface. *Advances in Water Resources* **25**, 1017–1042 (2002).

- 582 [21] Song, J., Zhang, Y., Zhang, C., Du, X., Guo, Z., Kuang, Y., Wang, Y., Wu, P., Zou, K., Zou, L. & Lv,
583 J. A microfluidic device for studying chemotaxis mechanism of bacterial cancer targeting. *Sci Rep* **8**, 6394
584 (2018).
- 585 [22] Lee, J.H., Fredrickson, J.K., Plymale, A.E., Dohnalkova, A.C., Resch, C.T., McKinley, J.P. & Shi, L.
586 An autotrophic H₂-oxidizing, nitrate-respiring, Tc(VII)-reducing *Acidovorax* sp. isolated from a
587 subsurface oxic-anoxic transition zone: H₂-oxidizing, Tc-reducing *Acidovorax* spp. *Environmental*
588 *Microbiology Reports* **7**, 395–403 (2015).
- 589 [23] Caccavo Jr, F., Lonergan, D.J., Lovley, D.R., Davis, M., Stolz, J.F. & McInerney, M.J. *Geobacter*
590 *sulfurreducens* sp. nov., a hydrogen- and acetate-oxidizing dissimilatory metal-reducing microorganism.
591 *Appl Environ Microbiol* **60**, 3752–3759 (1994).
- 592 [24] Ahmed, B., Cao, B., McLean, J.S., Ica, T., Dohnalkova, A., Istanbullu, O., Paksoy, A., Fredrickson,
593 J.K. & Beyenal, H. Fe(III) Reduction and U(VI) Immobilization by *Paenibacillus* sp. Strain 300A, Isolated
594 from Hanford 300A Subsurface Sediments. *Appl Environ Microbiol* **78**, 8001–8009 (2012).
- 595 [25] Krawczyk-Bärsch, E., Gerber, U., Müller, K., Moll, H., Rossberg, A., Steudtner, R. & Merroun, M.L.
596 Multidisciplinary characterization of U(VI) sequestration by *Acidovorax facilis* for bioremediation
597 purposes. *Journal of Hazardous Materials* **347**, 233–241 (2018).
- 598 [26] Methé, B.A., Nelson, K.E., Eisen, J.A., Paulsen, I.T., Nelson, W., Heidelberg, J.F., Wu, D., Wu, M.,
599 Ward, N., Beanan, M.J. & Dodson, R.J. Genome of *Geobacter sulfurreducens*: Metal Reduction in
600 Subsurface Environments. *Science* **302**, 1967–1969 (2003).
- 601 [27] Govarthanan, M., Mythili, R., Selvankumar, T., Kamala-Kannan, S., Rajasekar, A. & Chang, Y.C.
602 Bioremediation of heavy metals using an endophytic bacterium *Paenibacillus* sp. RM isolated from the
603 roots of *Tridax procumbens*. *3 Biotech* **6**, 242 (2016).
- 604 [28] Jin, F., Conrad, J.C., Gibiansky, M.L. & Wong, G.C. Bacteria use type-IV pili to slingshot on
605 surfaces. *Proceedings of the National Academy of Sciences*, **108**(31), pp.12617-12622 (2011).
- 606 [29] Speers, A.M., Schindler, B.D., Hwang, J., Genc, A. & Reguera, G. Genetic identification of a PilT
607 motor in *Geobacter sulfurreducens* reveals a role for pilus retraction in extracellular electron transfer.
608 *Frontiers in microbiology*, **7**, p.1578 (2016).
- 609 [30] Grady, E.N., MacDonald, J., Liu, L., Richman, A. & Yuan, Z.C. Current knowledge and perspectives
610 of *Paenibacillus*: a review. *Microbial cell factories*, **15**, pp.1-18 (2016).
- 611 [31] Jayathilake, P.G., Li, B., Zuliani, P., Curtis, T. & Chen, J. Modelling bacterial twitching in fluid flows:
612 a CFD-DEM approach. *Scientific reports*, **9**(1), p.14540 (2019).
- 613 [32] Nakamura, S. Spirochete flagella and motility. *Biomolecules*, **10**(4), p.550 (2020).
- 614 [33] Bahar, O., De La Fuente, L. & Burdman, S. Assessing adhesion, biofilm formation and motility of
615 *Acidovorax citrulli* using microfluidic flow chambers. *FEMS Microbiology letters*, **312**(1), pp.33-39
616 (2010).

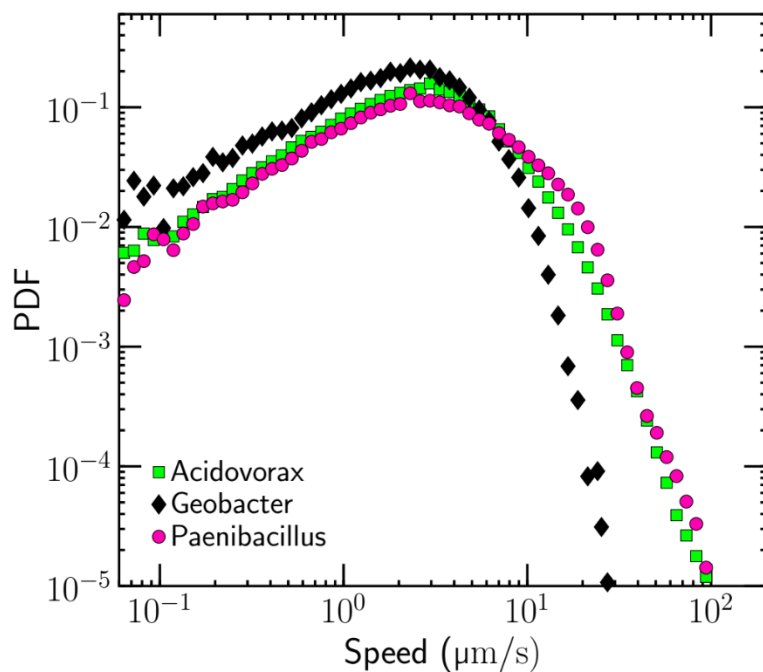
- 617 [34] Tinevez, J.Y., Perry, N., Schindelin, J., Hoopes, G.M., Reynolds, G.D., Laplantine, E., Bednarek, S.Y.,
618 Shorte, S.L. & Eliceiri, K.W. TrackMate: An open and extensible platform for single-particle tracking.
619 *Methods* **115**, 80–90 (2017).
- 620 [35] Yang, X., Parashar, R., Sund, N.L., Plymale, A.E., Scheibe, T.D., Hu, D. & Kelly, R.T. On Modeling
621 Ensemble Transport of Metal Reducing Motile Bacteria. *Sci Rep* **9**, 14638 (2019).
- 622 [36] Lovley, D.R., & Phillips, E.J.P. Novel mode of microbial energy metabolism: organic carbon oxidation
623 coupled to dissimilatory reduction of iron or manganese. *Appl. Environ. Microbiol.* **54**, 1472–1480 (1988).
- 624 [37] Plymale, A.E., Bailey, V.L., Fredrickson, J.K., Heald, S.M., Buck, E.C., Shi, L., Wang, Z., Resch,
625 C.T., Moore, D.A. & Bolton Jr, H. Biotic and Abiotic Reduction and Solubilization of Pu(IV) $O_2 \cdot xH_2O(am)$
626 as Affected by Anthraquinone-2,6-disulfonate (AQDS) and Ethylenediaminetetraacetate (EDTA). *Environ.*
627 *Sci. Technol.* **46**, 2132–2140 (2012).
- 628 [38] Thornton, M.M., Chung-Esaki, H.M., Irvin, C.B., Bortz, D.M., Solomon, M.J. & Younger, J.G.
629 Multicellularity and antibiotic resistance in Klebsiella pneumoniae grown under bloodstream-mimicking
630 fluid dynamic conditions. *The Journal of infectious diseases*, 206(4), pp.588–595 (2012).
- 631 [39] Tuval, I., Cisneros, L., Dombrowski, C., Wolgemuth, C.W., Kessler, J.O. & Goldstein, R.E. Bacterial
632 swimming and oxygen transport near contact lines. *Proceedings of the National Academy of Sciences*,
633 102(7), pp.2277–2282 (2005).
- 634 [40] Rossy, T., Nadell, C.D. & Persat, A. Cellular advective-diffusion drives the emergence of bacterial
635 surface colonization patterns and heterogeneity. *Nature communications*, 10(1), p.2471 (2019).
- 636 [41] Dehkharghani, A., Waisbord, N., Dunkel, J. & Guasto, J.S. Bacterial scattering in microfluidic crystal
637 flows reveals giant active Taylor–Aris dispersion. *Proceedings of the National Academy of Sciences*,
638 116(23), pp.11119–11124 (2019).
- 639 [42] Einstein, A. On the Movement of Small Particles Suspended in Stationary Liquids Required by the
640 Molecular-Kinetic Theory of Heat. *Annalen Der Physik*, 549–560 (1905).
- 641 [43] Duffy, K. J. & Ford, R. M. Turn angle and run time distributions characterize swimming behavior for
642 *Pseudomonas putida*. *J Bacteriol* **179**, 1428–1430 (1997).
- 643 [44] Berg, H.C. & Brown, D.A. Chemotaxis in *Escherichia coli* analysed by three-dimensional tracking.
644 *Nature*, 239(5374), pp.500–504 (1972).
- 645 [45] Becker, M. W., Metge, D. W., Collins, S. A., Shapiro, A. M. & Harvey, R. W. Bacterial Transport
646 Experiments in Fractured Crystalline Bedrock. *Ground Water* **41**, 682–689 (2003).
- 647 [46] Liu, J., Ford, R. M. & Smith, J. A. Idling Time of Motile Bacteria Contributes to Retardation and
648 Dispersion in Sand Porous Medium. *Environ. Sci. Technol.* **45**, 3945–3951 (2011).
- 649 [47] Dentz, M., Creppy, A., Douarche, C., Clément, E. & Auradou, H. Dispersion of motile bacteria in a
650 porous medium. *J. Fluid Mech.* **946**, A33 (2022).
- 651 [48] Conrad, J. C. & Poling-Skutvik, R. Confined Flow: Consequences and Implications for Bacteria and
652 Biofilms. *Annu. Rev. Chem. Biomol. Eng.* **9**, 175–200 (2018).

- 653 [49] Dehkharghani, A., Waisbord, N. & Guasto, J.S. Self-transport of swimming bacteria is impaired by
654 porous microstructure. *Commun Phys* **6**, 18 (2023).
- 655 [50] Ford, R.M. & Harvey, R.W. Role of chemotaxis in the transport of bacteria through saturated porous
656 media, *Advances in Water Resources* **30**(6-7): 1608-1617 (2008).
- 657 [51] Bente, K., Mohammadinejad, S., Charsooghi, M.A., Bachmann, F., Codutti, A., Lefèvre, C.T.,
658 Klumpp, S. & Faivre, D. High-speed motility originates from cooperatively pushing and pulling flagella
659 bundles in bilophotrichous bacteria. *Elife*, **9**, p.e47551 (2020).
- 660 [52] Najafi, J., Shaebani, M.R., John, T., Altegoer, F., Bange, G. & Wagner, C. Flagellar number governs
661 bacterial spreading and transport efficiency. *Sci Adv* **4**: eaar6425 (2018).
- 662 [53] Mitchell, J.G. The energetics and scaling of search strategies in bacteria. *The American Naturalist*,
663 **160**(6), pp.727-740 (2002).
- 664 [54] Kaya, T. & Koser, H. Direct upstream motility in Escherichia coli. *Biophysical journal*, **102**(7),
665 pp.1514-1523 (2012).
- 666 [55] Perez, L.J., Hidalgo, JJ., & Dentz, M. Upscaling of mixing-limited bimolecular chemical reactions in
667 Poiseuille flow. *Water Resources Research* **55**, no. 1: 249-269 (2019).
- 668 [56] Puyguiraud, A., Perez, L.J., Hidalgo, JJ., & Dentz, M. Effective dispersion coefficients for the
669 upscaling of pore-scale mixing and reaction. *Advances in Water Resources* **146**: 103782 (2020).
- 670 [57] Weber, S.C., Thompson, M.A., Moerner, W.E., Spakowitz, A.J., & Theriot, J.A. Analytical tools to
671 distinguish the effects of localization error, confinement, and medium elasticity on the velocity
672 autocorrelation function. *Biophysical journal*, **102**(11), 2443-2450 (2012).
- 674 [58] Weller, H. G., Tabor, G., Jasak, H. & Fureby, C. A tensorial approach to computational continuum
675 mechanics using object-oriented techniques. *Comput. Phys.* **12**, 620 (1998).
- 676 [59] OpenFOAM Foundation. OpenFOAM: Open-source CFD software. Retrieved from
677 <https://openfoam.org/> (2023).
- 678 [60] Vennamneni, L., Nambiar, S., & Subramanian, G. "Shear-induced migration of microswimmers in
679 pressure-driven channel flow." *Journal of Fluid Mechanics* **890**: A15 (2020).
- 680 [61] Lee, M., Lohrmann, C., Szuttor, K., Auradou, H. & Holm, C. The influence of motility on bacterial
681 accumulation in a microporous channel. *Soft Matter*, **17**(4), pp.893-902 (2021).
- 682 [62] Jeffery, G.B. The motion of ellipsoidal particles immersed in a viscous fluid. *Proceedings of the Royal
683 Society of London. Series A, Containing papers of a mathematical and physical character*, **102**(715), pp.161-
684 179 (1922).
- 685 [63] Pedley, T.J. & Kessler, J.O. Hydrodynamic phenomena in suspensions of swimming microorganisms.
686 *Annual Review of Fluid Mechanics*, **24**(1), pp.313-358 (1992).
- 687 [64] Choudhary, A., Paul, S., Rühle, F. & Stark, H. How inertial lift affects the dynamics of a
688 microswimmer in Poiseuille flow. *Communications Physics*, **5**(1), p.14 (2022).

- 689 [65] Yang, J., Kikuchi, K. & Ishikawa, T. High shear flow prevents bundling of bacterial flagella and
690 induces lateral migration away from a wall. *Communications Physics*, 6(1), p.354 (2023).
- 691 [66] Weiss, T.H., Mills, A.L., Hornberger, G.M. & Herman, J.S. Effect of bacterial cell shape on transport
692 of bacteria in porous media. *Environmental science & technology*, 29(7), pp.1737-1740 (1995).
- 693 [67] Fontes, D.E., Mills, A.L., Hornberger, G.M. & Herman, J. Physical and chemical factors influencing
694 transport of microorganisms through porous media. *Applied and Environmental Microbiology*, 57(9),
695 pp.2473-2481 (1991).
- 696 [68] F. Grant Ferris; Natalie Szponar; & Brock A. Edwards. *Groundwater Microbiology. The Groundwater*
697 *Project* (2021).
- 698 [69] Molaei, M. & Sheng, J. Succeed escape: Flow shear promotes tumbling of Escherichia coli near a solid
699 surface. *Sci Rep* **6**, 35290 (2016).
- 700 [70] Johnson, W. P., Blue, K. A., Logan, B. E. & Arnold, R. G. Modeling Bacterial Detachment During
701 Transport Through Porous Media as a Residence-Time-Dependent Process. *Water Resour. Res.* **31**, 2649–
702 2658 (1995).
- 703 [71] Dong, H., Scheibe, T. D., Johnson, W. P., Monkman, C. M. & Fuller, M. E. Change of Collision
704 Efficiency with Distance in Bacterial Transport Experiments. *Ground Water* **44**, 415–429 (2006).
- 705 [72] Hermansson, M. The DLVO theory in microbial adhesion. *Colloids and Surfaces B: Biointerfaces* **14**,
706 105–119 (1999).
- 707 [73] Licata, N.A., Mohari, B., Fuqua, C. & Setayeshgar, S. Diffusion of bacterial cells in porous media.
708 *Biophysical journal*, 110(1), pp.247-257 (2016).
- 709 [74] Alonso-Matilla, R., Chakrabarti, B. a& nd Saintillan, D. Transport and dispersion of active particles
710 in periodic porous media. *Physical Review Fluids*, 4(4), p.043101 (2019).
- 711 [75] de Anna, P., Pahlavan, A.A., Yawata, Y., Stocker, R. & Juanes, R.. Chemotaxis under flow disorder
712 shapes microbial dispersion in porous media. *Nat. Phys.* **17**, 68–73 (2021).
- 713 [76] Son, K., Brumley, D.R., & Stocker, R. Live from under the lens: exploring microbial motility with
714 dynamic imaging and microfluidics. *Nature Reviews Microbiology*. **13**, 761–775 (2015).
- 715 [77] Lu, N., Bevard, T., Massoudieh, A., Zhang, C., Dohnalkova, A.C., Zilles, J.L. & Nguyen, T.H.
716 Flagella-Mediated Differences in Deposition Dynamics for Azotobacter vinelandii in porous media.
717 *Environ. Sci. Technol.* **47**, 5162–5170 (2013).

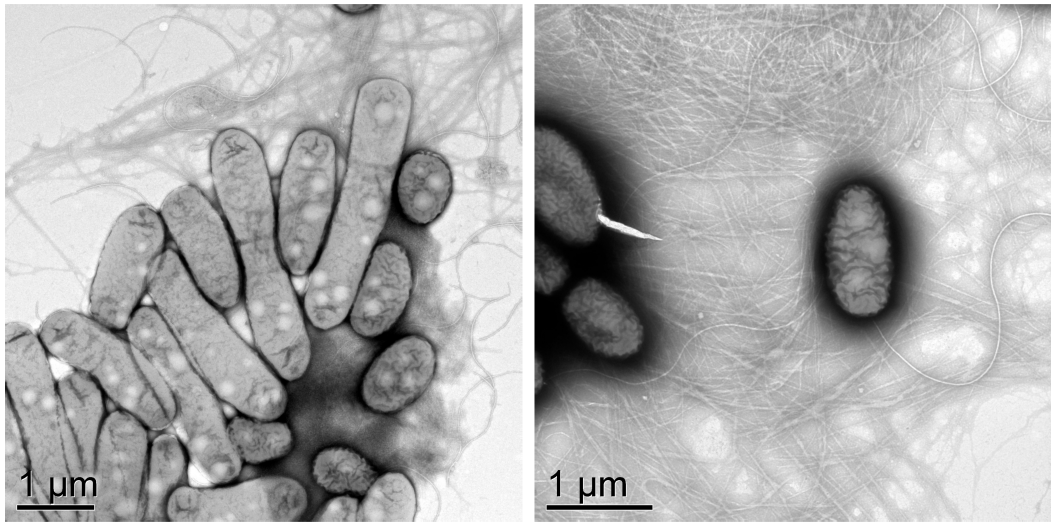
718 **Supplementary Figures**

719



720

721 **Supplementary Figure 1.** Speed PDF for no-flow experiments in the high porosity geometry (grain diameter = 40
722 μm , pore length = 20 μm).



723

724 **Supplementary Figure 2.** Whole-mount transmission electron microscopy (TEM) images of *Acidovorax* JHL-9
725 (unpublished images from [22], courtesy of Alice Dohnalkova). The whole-mount images were prepared by adding
726 JHL-9 liquid culture to a copper electron microscopy grid and examining by TEM at 200 kV using a JEOL 2010 high-
727 resolution TEM.